Torsional Ratcheting Actuating System

Stephen M. Barnes, Samuel L. Miller, M. Steven Rodgers, Fernando Bitsie

Sandia National Laboratories
MS 1080, PO Box 5800, Albuquerque, NM, 87185
smbarne@sandia.gov, (505)284-3310, fax: (505)844-2991, http://mems.sandia.gov/

1 ABSTRACT

A new type of surface micromachined ratcheting actuation system has been developed at the Microelectronics Development Laboratory at Sandia National Laboratories. The actuator uses a torsional electrostatic comb drive that is coupled to an external ring gear through a ratcheting scheme. The actuator can be operated with a single square wave, has minimal rubbing surfaces, maximizes comb finger density, and can be used for open-loop position control. The prototypes function as intended with a minimum demonstrated operating voltage of 18V. The equations of motion are developed for the torsional electrostatic comb drive. The resonant frequency, voltage vs. displacement and force delivery characteristics are predicted and compared with the fabricated device's performance.

Keywords: MEMS, Actuator, Electrostatic, Comb, Ratchet

2 INTRODUCTION

The development of actuation methods that meet the stringent requirements of MEMS applications has received limited attention, and is a critical need. Numerous types of MEMS actuators have been proposed based on electromagnetic, piezoelectric, thermal, and electrostatic principles [1]. However, many of these actuators display small displacement outputs, require complicated post-processing, are difficult to operate, and require large voltage inputs.

The goal of this work is to develop and characterize a reliable surface micromachined actuator that provides a significant force and displacement output with precise open loop positioning using simple low voltage drive signals. Electrostatic actuation is readily implemented in surface micromachining and is well characterized, so it was chosen to address this goal. The actuator presented herein is termed the torsional ratcheting actuator or TRA.

3 TORSIONAL RATCHETING ACTUATOR

The TRA uses rotational comb drives for electrostatic operation which are similar to previous gyro designs [2,3]. A large circular frame ties the movable banks of combs together. See Figure 1 for a SEM of the fabricated device. Four cantilever beams support this frame in its center and act as the frame's spring return. These four beams are resistant to any lateral motion of the frame but allow it to rotate. The frame is limited to 2.8º of rotation by stiff spring stops at its outside edge. To avoid stiction problems, the frame has dimples fabricated in its bottom surface to ensure the frame is physically separated from the underlying ground plane.

The torsion frame is surrounded by a 375µm radius ring gear which has standard involute gear teeth on its circumference that were designed to mesh with Sandia's standard MEMS components. Four overhanging clips hold it to the substrate and also constrain it to only rotational movement. The inside of the ring gear is lined with a rack of ratchet teeth that have a pitch of 13µm. Equally spaced around the edge of the torsion frame are three ratchet pawls that engage with the ratchet teeth. To prevent any unwanted reverse motion of the gear, there are three anti-reverse mechanisms that engage the ratchet teeth. The anti-reverse mechanisms are anchored cantilever beams that engage with the ratchet teeth.

To prevent electrostatic attraction to the underlying substrate, the frame is fabricated above a thin ground plane of polysilicon. The frame is connected to the ground plane at the central torsion springs. The stationary sections of the comb banks are connected using electrically isolated pieces of the ground plane. The interconnect to the stationary banks of combs is made using a signal line that passes above the gear and connects with one of the stationary comb banks.

To actuate the TRA, a periodic voltage signal is applied through this interconnect to the stationary combs. As the signal voltage increases, the torsion frame rotates counter-clockwise about its springs in response to the electrostatic attraction between the stationary and moving comb fingers. As the frame begins to rotate, the ratchet pawls engage the ring gear and cause it to also rotate. As the gear is rotating, the anti-reverse mechanisms are forced out of their engagement with the ratchet teeth and, once the ring gear has moved sufficiently, they reengage the next tooth. When the voltage is removed, the central torsion springs force the frame to return to its fabricated position. As the frame is returning, the ratchet pawls attempt to drag the ring gear in the reverse direction but the anti-reverse mechanisms have engaged and the ratchet pawls are forced to skip over the tooth and finally engage the next tooth. At this point, the frame has returned to its initial position, and the cycle can be repeated.

This type of actuator has many inherent advantages. One important feature of the actuator is its high density of electrostatic force elements. This high density is the result of a compact overall actuator layout. This density is important for applications because it minimizes the voltage required to drive a load while minimizing the area the actuator consumes on a die. Also, because the ring gear is only ratcheted in one direction, the TRA requires only two electrical connections to

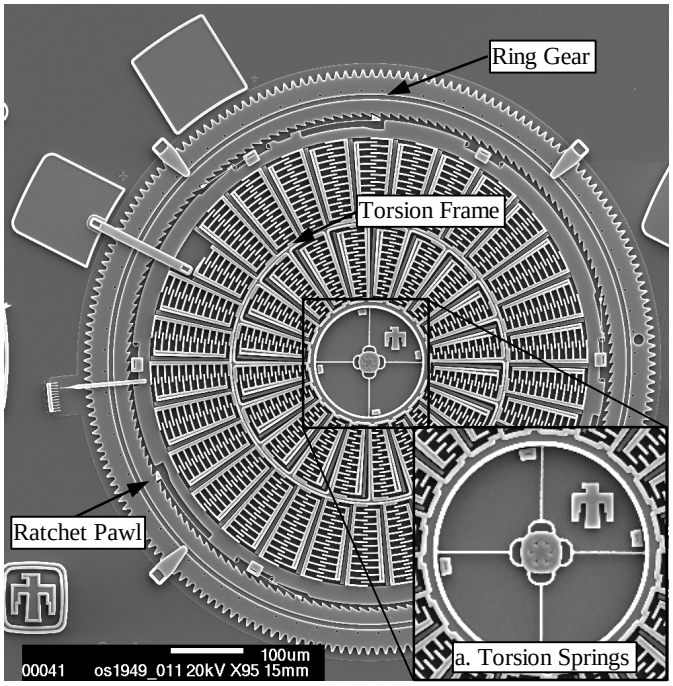

Figure 1. SEM of the fabricated torsional ratcheting actuator. a. shows an enlarged view of the central torsion springs.

run, and operates on extremely simple input signals. Finally, the use of a ratcheting system produces discrete displacement outputs. This is highly relevant because the actuator can be used for open loop positioning of a load.

4 THEORY

Model-based design parameters that will result in low voltage operation require appropriate system models. The torsion frame is the focus of the modeling presented here. The ring gear is not included in the model due to stiction and damping forces that are difficult to represent. The overall model for the torsion frame is obtained by summation of moments about its center torsion springs. This allows direct extraction of torque-displacement, voltage-displacement, and voltage-force relationships. The model for the system is based on:

$$T_{ic}(V,q)+T_{oc}(V,q)-T_s(q)=I\frac{d^2q}{dt^2} \qquad (1)$$

where T_{ic} is the torque produced by the inner banks of comb fingers, T_{oc} is the torque produced by the outer banks of comb fingers, T_s is the resisting torque of the center torsion springs, I is the moment of inertia of the torsion frame, θ is the angular displacement of the torsion frame, V is the applied voltage, and t is time.

To model the torque output of the combs, linear comb theory was combined with parallel plate theory [4]. This was done to account for the linear clamping of the comb banks that occurs at the end of each comb's travel. Summing the individual torque contributions of each comb finger yields:

$$T_{ic}(V,q)=bn\sum_{combs}\left[\left(\frac{A}{2g_t(q)^2}+\frac{h}{g_s}\right)\varepsilon rV^2\right] \qquad (2)$$

where n is the number of inner comb banks, A is the area of the tip of the comb, g_t is the parallel plate gap between the end of a finger and the root of the opposing comb, h is the vertical thickness of the combs, g_s is the gap between adjacent comb fingers, ε is the dielectric constant for air, and r is the radius of the individual comb finger. The β term in equation 2 accounts for the decrease in the capacitance of the electrostatic combs due to the underlying ground plane. Tang [5] shows this term can be approximately 0.7, which represents a 30% reduction in the force output of the combs. All calculations in this analysis use 0.7 for β. There is a similar expression for T_{oc}.

The torsion springs are not adequately described by linear beam theory. The end of each beam that makes up the torsion springs is forced to undergo an in-plane displacement along with an angular deflection. Also, while the torsion frame is rotating, the nearly clamped-clamped geometry of the torsion springs requires the individual beams to be stretched during the displacement. In an attempt to alleviate this strain and generate linear spring behavior, relief springs were placed at the root of each torsion beam.

Due to the complicated spring displacement and geometry, a three-dimensional non-linear finite element analysis (FEA) was performed to calculate their stiffness. The finite element model used was of a single cantilever and its strain relief structures. The boundary conditions used were deflection and angle specifications at the free end of the spring and fixed conditions at the base of the spring. I-DEAS was used to mesh the spring and Abacus was used to do the non-linear calculations. The total end moment required to deflect the beam to the end conditions was calculated at one degree displacements. A polynomial fit was then used to find the torque-deflection relationship:

$$T_s=149q+11.8q^2-1.65q^3 \qquad (3)$$

5 EXPERIMENTAL RESULTS

The TRA was fabricated in SUMMiT at the Microelectronics Development Laboratory at Sandia National Laboratories (see Figure 1). To conserve space, the fabrication details are omitted from this article and can be found in [6].

The fabricated devices demonstrated behavior as predicted from the models. Design variations produced minimum actuation voltages between 18V and 35V. The TRA has also shown to be very robust to larger voltage inputs. Up to 150V has been applied with no observed detrimental effects.

Initial lifetime tests have demonstrated up to 10^8 cycles to failure. This is equivalent to 600,000 gear revolutions. This number of actuation cycles drives the ring gear a linear distance of nearly 1.5 km. Also, initial testing has shown a

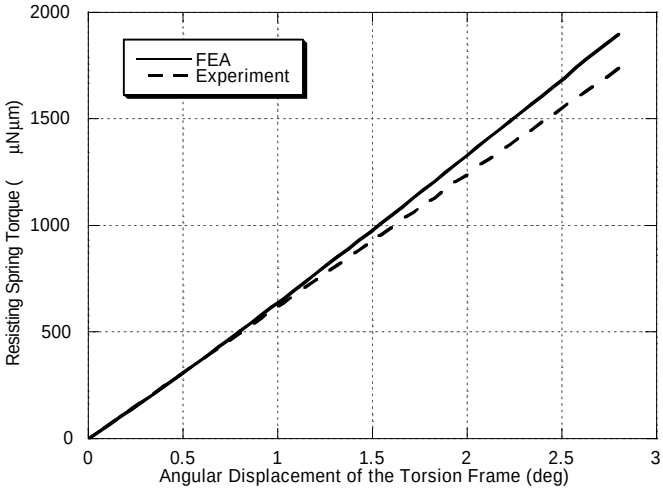

Figure 2. Resisting spring torque as a function of the angular displacement of the torsion frame. The FEA calculations are compared with the experimentally derived spring stiffness. The 'Experiment' curve was obtained by measuring the natural frequency of the torsion frame at one displacement and determining an "effective" stiffness.

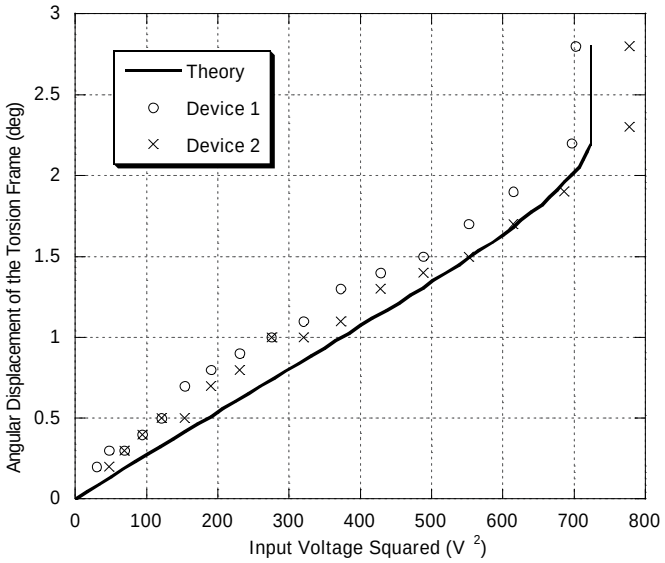

Figure 3. Comparison between the experimental and theoretical angular displacement of the torsion frame due to applied voltage.

greater than 90% yield of the unpackaged devices with no prior manipulation required.

In previous comb driven actuator designs [7], lateral clamping of the comb fingers was a serious issue. Lateral clamping is directly related to the lateral stiffness of the support springs and this spring design was chosen due to its inherent stiffness. Spiral springs were initially considered because simple models exist, but they were rejected due to their inherent vertical and lateral compliance. The stiffness of the torsion springs has contributed strongly to the TRA's robustness to release and over-voltage.

The type of signal that is used to drive the TRA affects the ratcheting performance of the device. This is due to the relatively large inertia of the ring gear. If a pure square wave is applied to the combs, the strong impulse that is given to the ring gear can impart enough momentum to cause the gear to move past multiple ratchet steps. If a signal with a slower initial rise time is used, the gear is only moved one step. A triangle wave has shown to work well for driving the TRA.

Because the torsion springs are an important parameter in the models, their widths were measured using SEM. The springs showed clean definition and were approximately 80nm thinner than defined. This type of close match is required for the FEA analysis to be accurate because the stiffness of cantilever beams is typically related to the width of the springs cubed [8].

The natural frequency of the device at atmospheric pressure and temperature was measured by applying a low frequency square wave signal and observing its dynamic behavior using stroboscopic illumination. This allowed recording the torsion frame's free oscillations in a known time. This was performed on TRAs that did not have ratchet pawls so that the torsion frame was not making contact with the ring gear. The measured natural frequency of the torsion frame was 3800Hz. The FEA predicts a slightly faster response of approximately 3900 Hz. Using the measured natural frequency, a linear torsional spring constant was calculated for the device. This was done using a calculated moment of inertia of the torsion frame and assuming a linear spring response. Figure 2 shows the force-displacement response of the torsion springs as calculated by FEA and experiment. The FEA results match with the experimental measurement quite well and show a slight spring stiffening as the frame is displaced.

The frame's angular displacement response to voltage was also measured. DC signals from 0V to 30V were applied and the steady state angular displacement of the frame was recorded for each. The frame's displacement was measured using a pointer fabricated on the outside edge of the frame that indicates the frame's angular displacement in degrees. This pointer gives a 0.25° resolution because of the large outside radius of the TRA. These data are plotted against the theoretical response in Figure 3. As the figure shows, the theory predicts the electrostatic pull-in of the torsion frame to within 1V.

Finally, a measurement of the device's force output against voltage was done. To accomplish this, some of the devices were fabricated with folded springs attached as shown in Figure 4. The folded springs are attached to a linear gear rack that connects to the TRA's ring gear. A small periodic voltage was applied and the displacement amplitude of the folded springs was observed using a gauge fabricated on the springs. The displacement of the springs was recorded at each amplitude of the input signal. Using linear beam theory, the spring constant of the test structure was calculated. Using the displacement data and spring constant calculation, the force output was experimentally determined. The results of the experiment are shown in Figure 5.

In equation 2, it can be seen that the torque output of the comb banks depends on the voltage applied but also on the displacement of the frame. This is due to the parallel plate attraction of the ends of the comb fingers as they further engage with the opposing combs. Because of this

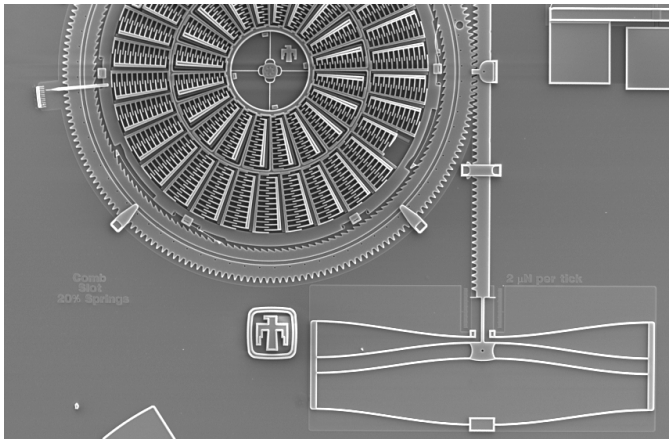

Figure 4. SEM of the force test structure after the experiment was performed. Note that the beams are held in the deflected position due to the action of the anti-reverse mechanisms. The beams have a stiffness of approximately 1μN/μm.

dependence, there is a range of possible force outputs for each applied voltage. The minimum and maximum force outputs for the voltage range were calculated from equation 1 and are plotted in Figure 5. The predictions bound the experimental results well.

6 CONCLUSIONS

We have designed and fabricated a new type of electrostatic actuator based upon ratcheting small angular displacements to allow significant force output with a discrete displacement output. The TRA has demonstrated reliable actuation and usable force at small voltages using very simple input signals. A dynamic model of the TRA has been developed and shown to accurately match the measured behavior of the fabricated devices. The model predicts the voltage requirements for actuation of the TRA to within 1V and accurately bounds the force output of the device.

One objective of the TRA design is low voltage operation. The system model was developed to address this objective by predicting the voltage response of the fabricated devices. As the model has been demonstrated to be accurate, improved designs can now be confidently developed. In order to achieve a higher force to voltage ratio, the fundamental actuation method of the TRA may be changed. This is the reason a full dynamic model was generated. Other actuation methods that are based on the dynamic behavior of the TRA could be used to dramatically reduce the voltage requirements. New designs are being considered which use resonant mode actuation and reverse mode actuation. In reverse mode actuation, the comb banks are used to initially displace the center torsion springs. This stored energy is then released to ratchet the ring gear and load. Additionally, the inertia of the torsion frame can be exploited in this mode to achieve larger initial frame/spring displacements than the steady state voltage would allow. To confidently design both the resonant mode and reverse mode actuators, this full dynamic model is required.

The torsional ratcheting actuator has demonstrated many desirable features as a MEMS actuator. Its size, simplicity of

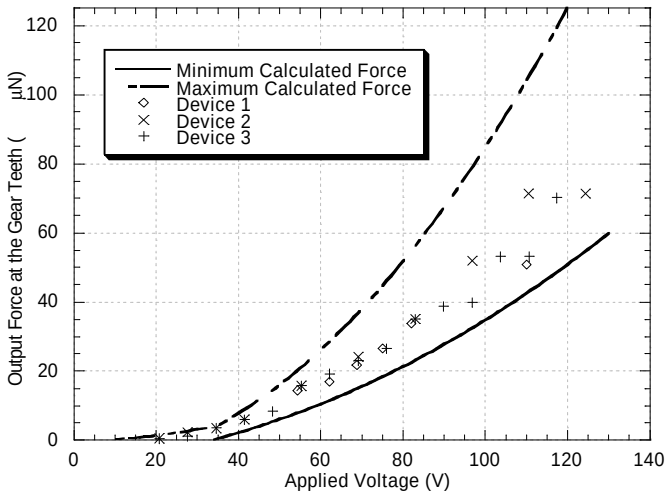

Figure 5. Comparison between the measured force output of the TRA with the maximum and minimum calculations. The particular TRAs used in this test had springs twice as stiff as the TRAs tested in Figure 3.

operation, and use in open loop control applications could make it a commonplace actuator design in MEMS.

Sandia is a multiprogram laboratory operated by Sandia Corporation, a Lockheed Martin Company, for the United States Department of Energy under Contract DE-AC04-94AL85000.

7 REFERENCES

[1] H. Fujita, H Toshiyoshi, "Micro actuators and their applications", Microelectronics Journal 29, 1998, pp. 637-640

[2] W. Geiger, B. Folkmer, U. Sobe, H. Sandmaier, W. Lang, "New designs of micromachined vibrating rate gyroscopes with decoupled oscillation modes", Sensors and Actuators A 66, 1998, pp. 118-124

[3] S. An, Y.S. Oh, K. Y. Park, S. S. Lee, C. M. Song, "Dual-axis microgyroscope with closed-loop detection", Sensors and Actuators 73, 1999, pp. 1-6

[4] J. J. Sniegowski, E. J. Garcia, "Microfabricated Actuators and Their Application to Optics", Proc. SPIE Miniaturized Systems with Micro-Optics and Micromechanics, 2383, 1995, pp. 46-64.

[5] W. Tang, "Electrostatic Comb Drive for Resonant Sensor and Actuator Applications", University of California at Berkeley, 1990, pp. 15

[6] J. J. Sniegowski, M. S. Rodgers, "Multi-layer enhancement to polysilicon surface micromachining technology", IEDM Tech. Digest, pp. 903-906, 1997

[7] E. J. Garcia, J. J. Sniegowski, "Surface Micromachined Microengine", Sensors and Actuators A 48, 1995, pp. 203-214.

[8] W. C. Young, Roark's Formulas for Stress & Strain, 6th Ed., Chap. 7, McGraw-Hill, Inc., New York, 1989, pp. 100